Analysis of Coherence and Coupling in Vertical Cavity Surface Emitting Laser Arrays

Pawel J. Strzebonski, William North, Nusrat Jahan, *Graduate Student Member, IEEE*, and Kent D. Choquette, *Fellow, IEEE*

(Invited Paper)

***Abstract*— The optical coupling between dual elements of photonic crystal vertical cavity surface emitting laser arrays is characterized. The optically coupled microcavity lasers have independent bias injection currents. Output power and beam analysis measurements are used to quantify the effects of optical coherence in nominally 850 nm emitting arrays. Modelling and experiment show how the optical coupling is influenced by photonic crystal lattice period and the independent current injection into the elements.**

***Index Terms*— Laser modes, optical coupling, phased arrays, semiconductor laser arrays, vertical-cavity surface emitting lasers (VCSEL).**

I. Introduction

COHERENTLY coupled two-element arrays of photonic crystal (PhC) vertical cavity surface emitting lasers (VCSELs) have been shown to exhibit novel dynamic properties such as increased small-signal modulation bandwidth [1], [2], enhanced digital data transmission [3], and reduced intensity noise and harmonic distortion [4]. These properties make them attractive for next-generation optical communications systems, however the modulation enhancement is dependent on the engineering of the array structure to enable effective optical coupling as well as the electrical tuning of the bias injection currents to operate at the prerequisite coherently coupled regime. These require developing the theory and model to understand the coupling behavior and the link between the array design and coupling, as well as developing the experimental methods to characterize these devices and tune them into coherence.

Past theoretical analysis of coupled VCSEL arrays has primarily involved one-dimensional real refractive index waveguide models [5] for the analysis of the array modes and their (real) coupling coefficient, and coupling coefficient formulations of the laser rate equations for the analysis of dynamics [6], [7]. A recently developed two-dimensional complex index waveguide model improves on past work by enabling the calculation of the complex coupling coefficient as a function of physical array structure [8] and is used here.

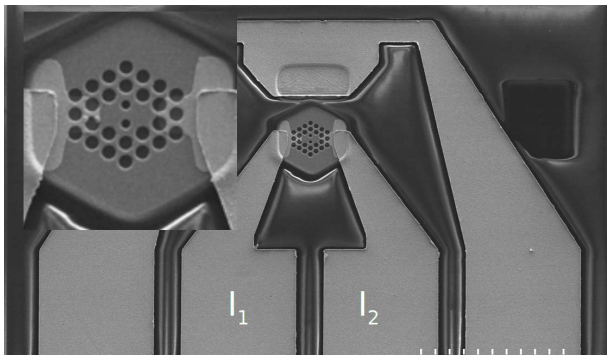

Fig. 1. SEM image of a 2 × 1 PhC VCSEL array with inset of magnified cavity.

Many different methods of coupled VCSEL array characterization have been previously proposed with relative strengths and weaknesses [9]. One recently proposed method is a Fourier-method beam profile analysis [9] that can provide insight into the array coupling, lasing mode suppression ratio, and inter-cavity phase difference in a simple but resilient manner [10]. Another is optical power analysis that exploits the coherent power enhancement effect to estimate the imaginary coupling coefficient from the strength of the power enhancement effect [7] using either conventional modeling techniques [11], [12] or machine learning methods [13].

In this work we use output power and beam analysis to quantify the effects of coherence for photonic crystal VCSEL arrays. We use optical power analysis on a collection of PhC VCSEL arrays and show the relation between the photonic crystal period and the magnitude of imaginary coupling coefficient, as well as its trends with increased injection current. We use Fourier-method beam profile analysis for determination of coherent coupling and demonstrate array supermode transitions with increase driving current. We adapt our previously proposed two-dimensional complex index waveguide model to experimental VCSEL arrays by fitting the model

Manuscript received 4 December 2021; revised 16 January 2022; accepted 21 January 2022. Date of publication 4 February 2022; date of current version 28 July 2022. This work was supported in part by the Office of Naval Research under Award N6833520C0927. *(Corresponding author: Pawel J. Strzebonski.)*

Pawel J. Strzebonski was with the Electrical and Computer Engineering Department, University of Illinois at Urbana-Champaign, Urbana, IL 61801 USA. He is now with II-VI Inc., Saxonburg, PA 16056 USA (e-mail: strzebo2@illinois.edu).

William North, Nusrat Jahan, and Kent D. Choquette are with the Electrical and Computer Engineering Department, University of Illinois at Urbana-Champaign, Urbana, IL 61801 USA.

Color versions of one or more figures in this article are available at https://doi.org/10.1109/JQE.2022.3149143.

Digital Object Identifier 10.1109/JQE.2022.3149143

TABLE I
NOMINAL DESIGN PARAMETERS FOR THE PHC STRUCTURE OF 2 × 1 VCSEL ARRAYS [17]

Design #	PhC Period	PhC Fill-Factor
1	4 μm	60%
2	4.5 μm	60%
3	5 μm	60%

parameters to match experimental estimates of imaginary coupling coefficient. Finally our complex waveguide model predicts supermode transitions with increased injection current (decreasing cavity index) consistent with the array measurements.

P. Daniel Dapkus submitted his doctoral thesis on characterization of laser operation from amphoterically doped GaAs in 1970 at the University of Illinois [14]. He continued III-V semiconductor and optoelectronic device research during his long and distinguished career overlapping both industry and academia. A half century later we follow his pioneering work and leverage many of his foundational discoveries to report on the lasing characteristics of more complexly structured, but essentially doped (Al)GaAs semiconductors.

II. PHOTONIC CRYSTAL VCSEL ARRAYS

Nominally symmetric two-element photonic crystal VCSEL arrays such as shown in Fig. 1 have been previously fabricated [2] and are characterized in this work. The conventional VCSEL epitaxy for 850 nm emission that is used is grown by metal organic chemical vapor deposition [15]. The photonic crystal patterns are defined using conventional optical lithography and etched into the top distributed Bragg reflector mirror using anisotropic etching. The dual array elements are defined by a missing hole in the photonic crystal and are electrically isolated by ion implantation with an independent electrical contact [2] as depicted in Fig. 1.

The photonic crystal pattern has been shown to influence the modal properties of individual photonic crystal VCSELs [16]. Here we focus on three array designs with varying period but fixed fill factor (ratio of hole diameter to period). Each cavity has a gain area defined by an ion implanted aperture with an optical aperture defined by the inner edge of the holes surrounding the defect cavity; thus the cavity diameter is twice the period with hole diameter subtracted. As is evident in the inset of Fig. 1, the inner two holes between the dual elements have reduced diameter to enhance coupling [17]. Three photonic crystal designs are considered with photonic crystal period of 4.0, 4.5, and 5.0 μm. With reduced period length, the cavity diameter and separation between the cavities also are reduced. The nominal design parameters for the photonic crystal VCSEL arrays are listed in Table I.

The photonic crystal VCSEL arrays were characterized at the wafer-level using unpackaged arrays with cascade contacts as shown in Fig. 1. The two electrically independent lasers were driven continuous wave using a separate precision source-measure instrument. The output power and far-field beam profile measurements were obtained separately from multiple arrays of each of the three photonic crystal designs. For the beam profile measurements, the optical train was set on a computer-controlled linear stage that enabled adjustment of the position of the focal plane in order to capture a beam image of the far-field. The VCSEL array behavior and performance is strongly dependent on the operating conditions, and thus we must characterize these devices across a wide range of driving currents and often with small current steps (e.g. 10 μA). Computer-controlled automated data collection was used to collect the data sets to be discussed next.

III. OPTICAL POWER ANALYSIS

The total optical power emitted by an array was measured across a range of injection currents to the two independent cavities. These automated power measurements are made for a collection of neighboring arrays for each of the three array designs. A representative example of the output power versus injection currents I_1 and I_2 are shown in Fig. 2a, 3a, and 4a for array designs # 1, 2, and 3 respectively. For each array type, we observe performance variations even for neighboring arrays, but several characteristics are consistently observed. We find each element has approximately equal threshold current, the output power generally increases with increasing current, where the power emitted from each element simply adds together.

The key feature of these optical power measurements is the "coherent ridge" features that tends to occur close to the equal-injection diagonal (where $I_1 \approx I_2$) of Fig. 2-3. The excess output power observed along the coherent ridge is a region where the optical power is greater than the sum of the element laser powers when operated individually. This phenomena occurs because the coherent optical array supermode has better confinement with the gain region than the individual cavity modes [7]. This ridge is consistently more prominent in design # 1 arrays (Fig. 2a) as compared to design # 2 arrays (Fig. 3a), and is barely discernible in design # 3 arrays (Fig. 4a).

Past work has shown that the strength of power enhancement is related to the magnitude of the imaginary coupling coefficient, $|\kappa_i|$ [7]. In order to extract the imaginary coupling coefficient from the coherent ridge measurements, we need to estimate the output power in the absence of lasing operation of the coherent supermode. The estimation of uncoupled power is nontrivial as accurate estimates need to incorporate thermal cross-talk effects (for example, where the heat from cavity 2 increases the threshold current thus decreases optical power in cavity 1). Past work has explore multi-variable polynomial modeling [9], artificial neural network modeling [9], [13], as well as single-variable polynomial modeling [10], [11]. In this work we use a two-step refining single-variable polynomial model evaluated separately on each one-dimensional slice of the optical power measurement data [10].

We determine the uncoupled optical power and optical power enhancement for each of the characterized arrays to estimate the magnitude of the imaginary coupling coefficient. The result of this analysis applied to the data sets for the representative arrays, is shown in Fig. 2b, 3b, and 4b for photonic crystal designs # 1, 2, and 3, respectively. Comparison of output power and the extracted value of plots in

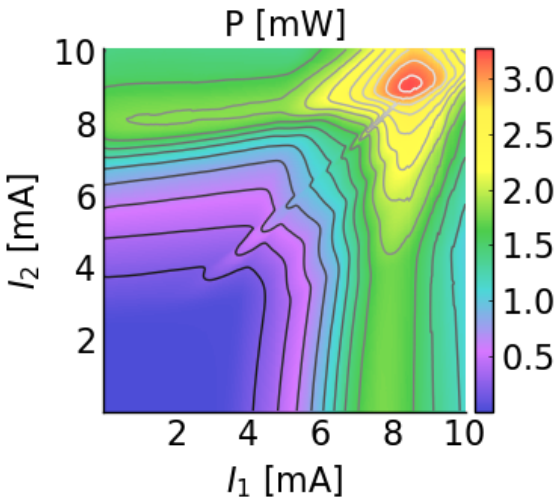

(a)

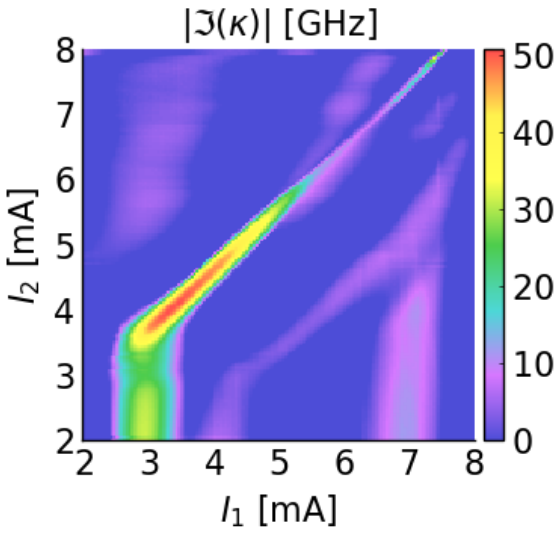

(b)

Fig. 2. Optical power measurement and estimated imaginary coupling coefficient of a design # 1 array.

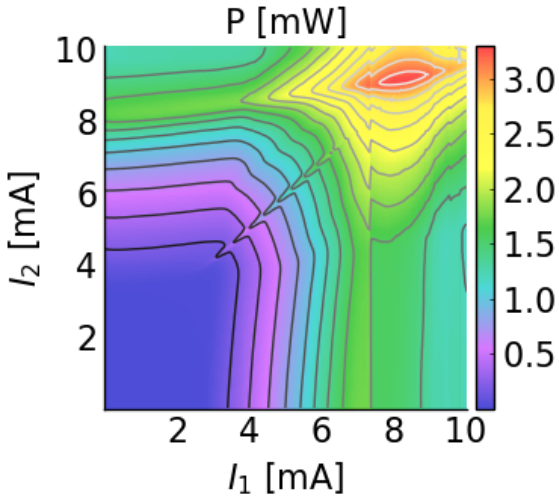

(a)

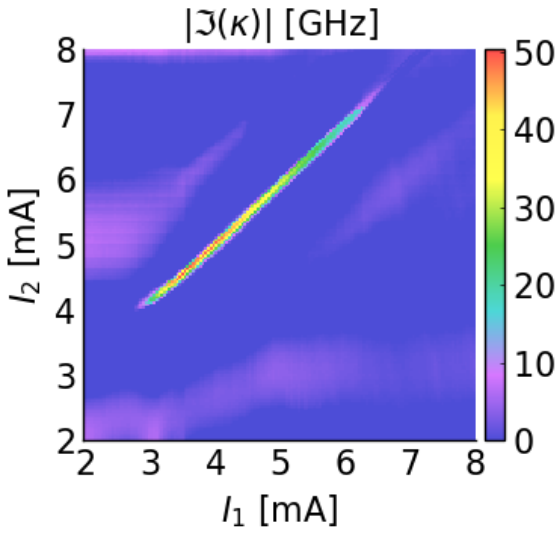

(b)

Fig. 3. Optical power measurement and estimated imaginary coupling coefficient of a design # 2 array.

Fig. 2, 3, 4 illustrates that the latter plots distinctly reveal the coherent ridge, even in Fig. 4b corresponding to photonic crystal design # 3. For every photonic crystal array data set collected, extracting the excess power produced from nearly degenerate supermodes when the array is biased in the power ridge under approximately equal-injection condition, distinctly highlights coherent operation of the array.

If we consider the magnitude of $|\kappa_i|$ along the coherent ridge with increasing current, we find that $|\kappa_i|$ tends to reach a maximum at not much above threshold, before decreasing to a relative minimum, as has been previously reported [7]. In some cases, as in Fig. 2b, $|\kappa_i|$ will increase with current toward a second maximum. The minimum value of $|\kappa_i|$ has been identified with a transition from one array supermode to another [11]. Past experimental analysis of the imaginary coupling coefficient showed estimated maximal values of 150 GHz [7].

While the arrays of a particular design should nominally be identical, the optical power measurements and analysis show significant variation in the optical power performance and coupling between distinct arrays of the same design. In order to compare the coupling as a function of PhC lattice period, we find the maximal estimated $|\kappa_i|$ for each measured array and plot as a function of photonic crystal period in Fig. 5. While the $|\kappa_i|$ can vary by a factor of ~ 2 within a given design, the average value of $|\kappa_i|$ shows a distinct trend of

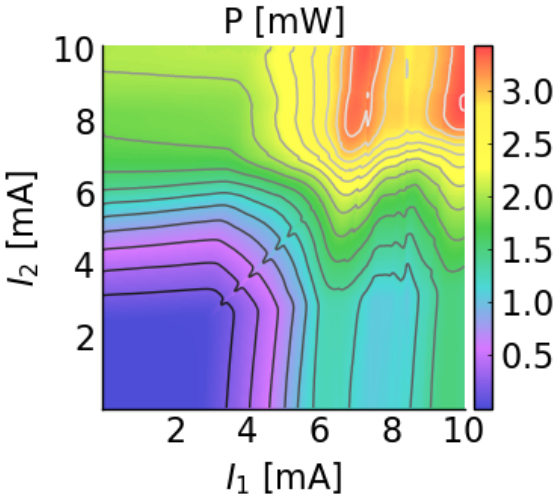

(a)

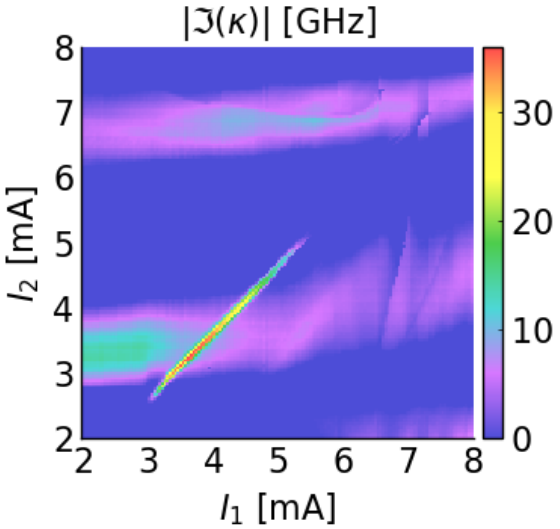

(b)

Fig. 4. Optical power measurement and estimated imaginary coupling coefficient of a design # 3 array.

decreasing $|\kappa_i|$ with increased PhC lattice period, a trend consistent with prior waveguide model results [8].

IV. Beam Profile Analysis

The beam profile of the photonic crystal laser arrays tend to develop interference fringes when the elements are coherently coupled. These fringes form the basis of beam profile analysis [9]. We measure the far-field beam profiles of the representative photonic crystal design # 1 array (see Fig. 2) at various injection currents in the vicinity of the coherent ridge. The beam profiles are then analyzed using the Fourier-method [9], [10] where the fast Fourier transform (FFT) is calculated for the beam intensity profile, and the value of the highest-magnitude (non-zero-frequency) side-peak in the FFT

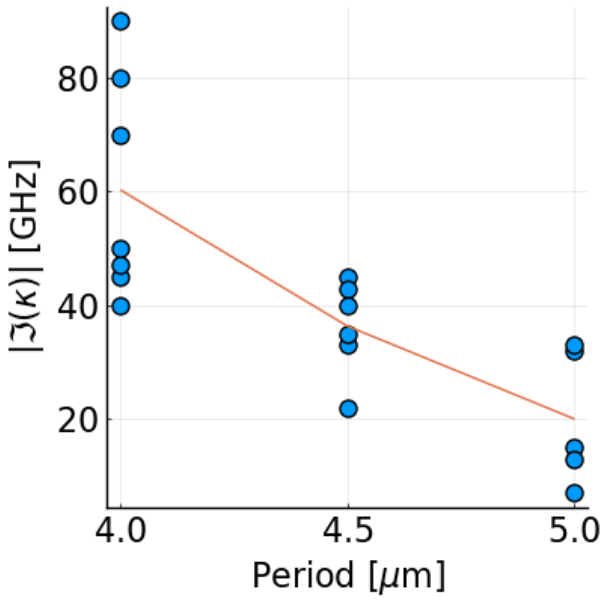

Fig. 5. Estimated peak imaginary coupling coefficient as a function of PhC lattice period. Average value is drawn in as curve.

is divided by the zero-frequency component. The magnitude of this ratio is the "peak ratio" and the phase of this ratio is referred to as the "peak phase". The calculated Fourier "peak ratio" metric and "peak phase" are plotted in Fig. 6a and 6b, respectively. The peak ratio, which ideally varies from 0 (uncoupled lasers) and 0.5 (fully coupled lasers), distinctly shows the coherent ridge as two regions of high peak ratio. Comparing Fig. 2b and 6a suggests the lower current region corresponds to the discernible coherent ridge and the second high peak ratio region (at higher current) corresponds to where the coherent ridge should appear, if it were discernible from optical power measurements.

The Fourier peak phase, plotted in Fig. 6b, corresponds to the relative phase of the supermode field in the two cavities. We can discern two primary trends in Fig. 6b. First, perpendicular to the coherent ridge ($I_1 \propto -I_2$) but within the coherent region the phase has a smoothly varying gradient, indicating beam-steering and non-Hermitian modes [18], [19]. Second, at higher currents along the coherent ridge ($I_1 \propto I_2$) the phase tends to be relatively constant except in the region of low $|\kappa_i|$ and low peak ratio at approximately $(I_1, I_2) = (4.5, 5.2)$, where a discontinuity of approximately 180° is found, as would be expected for a transition from one array supermode to the other [12].

We can better understand the supermode behavior by looking at a selection of far-field beam profiles such as shown in Fig. 7. Three sets of beam profiles are compared; the specific current ranges in Fig. 7a, 7b, and 7c are depicted in Fig. 6. First consider the profiles taken across the lower and upper coherent regions in Fig. 7a and 7b, respectively. Both sets show some beam-steering, but the steering per unit of current change is stronger in the upper coherent region [18]. Furthermore, the lower coherent region exhibits four-lobed out-of-phase supermode profile, while the upper coherent

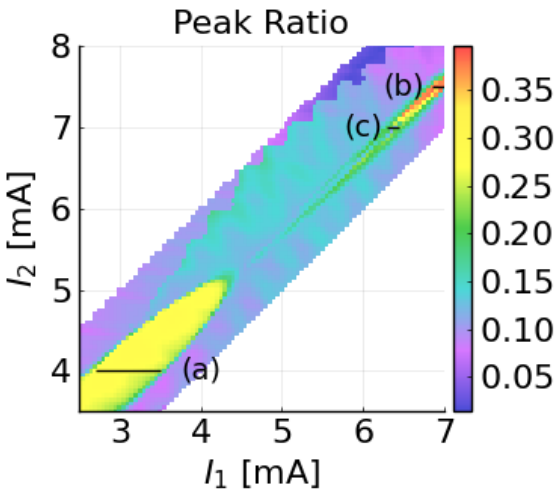

(a)

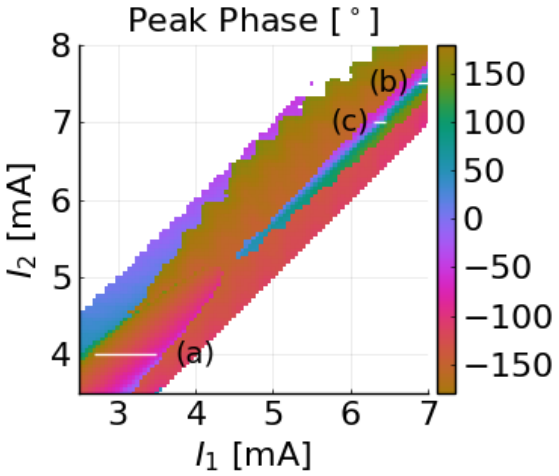

(b)

Fig. 6. Fourier beam analysis of design # 1 VCSEL array, with the 6a Fourier peak ratio and 6b Fourier peak phase metrics.

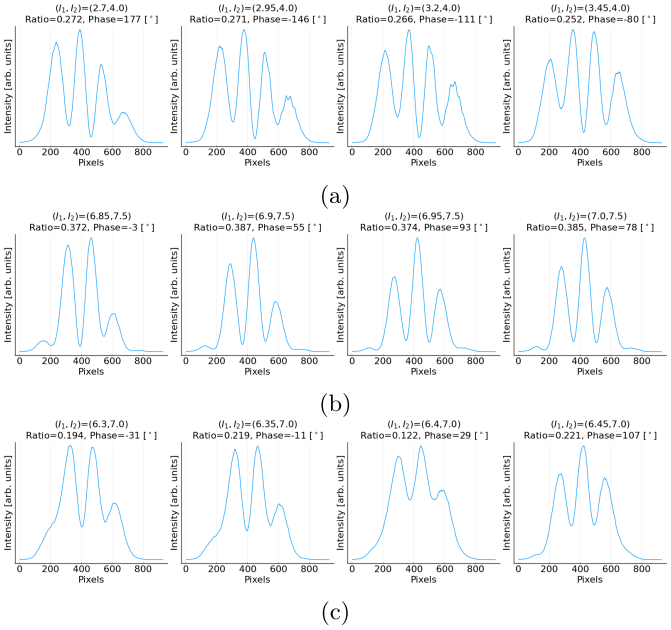

(a)

(b)

(c)

Fig. 7. Select beam intensity profiles from a design # 1 VCSEL array. 7a shows beam-steering at the low-power coherent ridge, 7b shows beam-steering at the high-power coherent ridge and 7c shows a transition from an out-of-phase-like beam to an in-phase-like beam with a dip in visibility at the bottom of the higher-power coherent ridge. The locations of these beam profiles on the peak ratio ridge are marked in 6a.

TABLE II

WAVEGUIDE MODEL PARAMETERS FOR A DESIGN # 1 2 × 1 VCSEL ARRAY. POSITIVE IMAGINARY INDEX INDICATES LOSS, NEGATIVE GAIN

Parameter:	Symbol:	Value:
Wavelength	λ_0	850 nanometers
Bulk index	n_{bulk}	$3.451 + 1.968 \times 10^{-3}i$
Index suppression	Δn	2.948×10^{-3}
Core index	n_{core}	$3.448 - 5.669 \times 10^{-4}i$
Hole index	n_{hole}	$1.844 + 1.968 \times 10^{-3}i$
PhC period	Λ	4 μm
PhC fill-factor	FF	0.6

region has a three-lobed in-phase supermode, in agreement with the phase transition appearing in Fig. 6b.

Another phenomenon observed in the beam profile analysis are regions of lowered Fourier peak ratio within coherent ridges. Consider the series of beam profiles in Fig. 7c. While all of the beam profiles are of moderate coherence, the third beam profile in this series (6.4 mA, 7.0 mA) has significantly lower coherence (peak ratio). The Fourier beam profile analysis predicts lowered peak ratio as optical coupling diminishes (development of asymmetric cavity modes) and reduction of mode suppression ratio [17]. Breaking optical coupling is expected at the outer edges of a coherent ridge, not along its diagonal center. Thus lower peak ratio within coherent ridges can be identified with regions of lowered mode suppression ratio.

V. MODELING AND THEORY

We build on the previously proposed waveguide model of VCSEL arrays [8] by adjusting the model parameters to fit experimental device performance. The photonic crystal parameters are given Table I. The complex imaginary index values for use in the waveguide model were fit to match the measured (average) imaginary coupling coefficients extracted from the three photonic crystal designs. This, however, implies that our parameter fitting is under-constrained as the waveguide model has three real index parameters and two imaginary index parameters, but we are fitting to only three experimental values. The derived model parameters, listed in Table II, are thus not unique and need additional refinement.

We use the parameters in Table II to create a complex index waveguide structure corresponding to the photonic crystal, such as illustrated in Fig. 8. Note the calculation domain

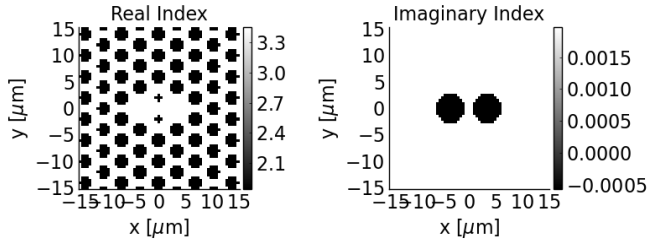

Fig. 8. Refractive index structure for a 2×1 VCSEL array waveguide model.

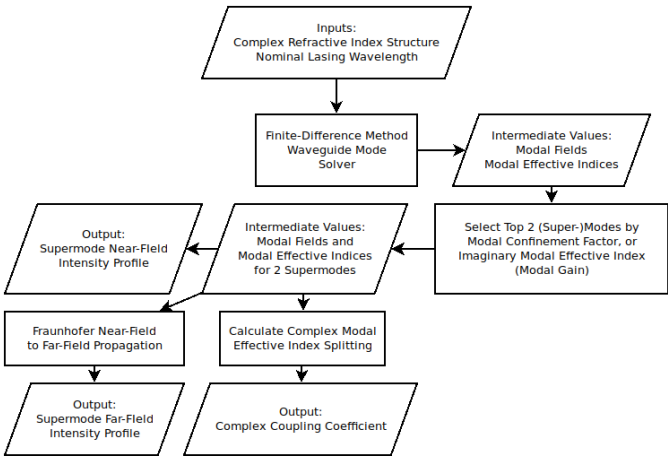

Fig. 9. Process flow diagram for waveguide modeling and coupling coefficient calculation.

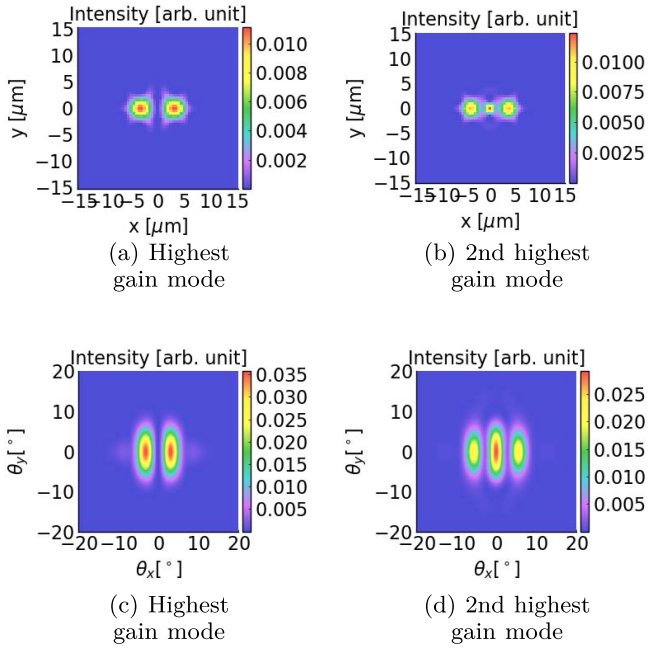

Fig. 10. 10a and 10b Mode intensity profiles for modes with highest confinement factors for a 2×1 VCSEL array waveguide model, and 10c and 10d their corresponding far-field intensity profiles.

in Fig. 8 accounts for the effects of the etched photonic crystal and carrier index suppression (but does not include thermal effects). A scalar waveguide eigenmode solver is used

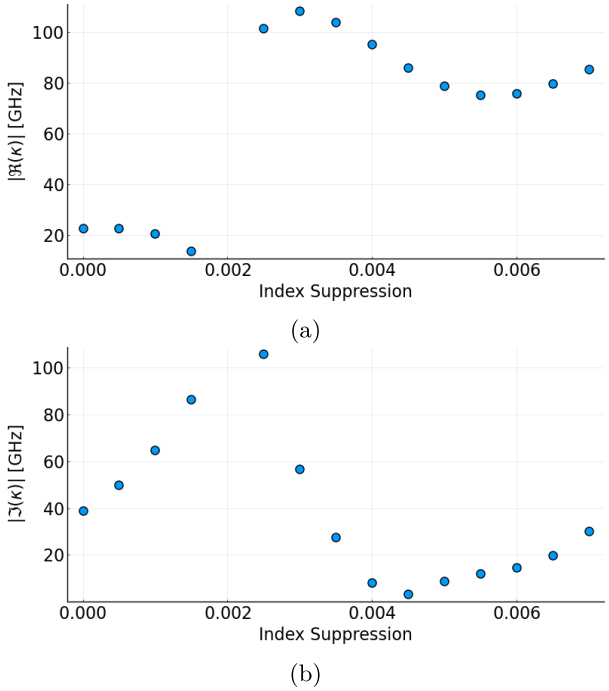

Fig. 11. Real and imaginary coupling coefficient for 2×1 VCSEL array as a function of cavity index suppression.

to find the modal fields with the highest confinement factor, that is supermodes with the greatest proportion of the modal power contained within the gain area of the array. We find a pair of dominant supermodes (e.g. in-phase and out-of-phase mode). The complex coupling coefficient is estimated using the complex modal effective indices for the two supermodes and is primarily determined by the difference between the modal effective indices for the two supermodes. The imaginary component of the modal effective index incorporates the gains and losses experienced by the mode, and as such the imaginary coupling coefficient is related to the gain splitting and difference in threshold gain for the two supermodes. This gain and threshold splitting is driving force behind the power enhancement effect [7] that we use to estimate the imaginary coupling coefficient. The intensity profiles for the primary and secondary array supermodes as well as the calculated beam profiles using Fraunhofer diffraction [18] are illustrated in Fig. 10. This modeling process flow is summarized in Fig. 9 and the details of the complex coupling coefficient estimation have been previously detailed [8].

With this model we can explore the effects of (symmetric) current injection into the two cavities. We presume the primary effect of current injection in the waveguide model is index suppression in the cores of the waveguides, with higher injection leading to stronger index suppression [20]. The calculated complex coupling coefficient derived from the splitting in the modal effective index for the two array supermodes [21] with increased index suppression (corresponding to increased current injection) is plotted in Fig. 11. Fig. 11b illustrates the imaginary component has an initial increase in $|\kappa_i|$, followed by a drop toward zero, and a subsequent increase. These

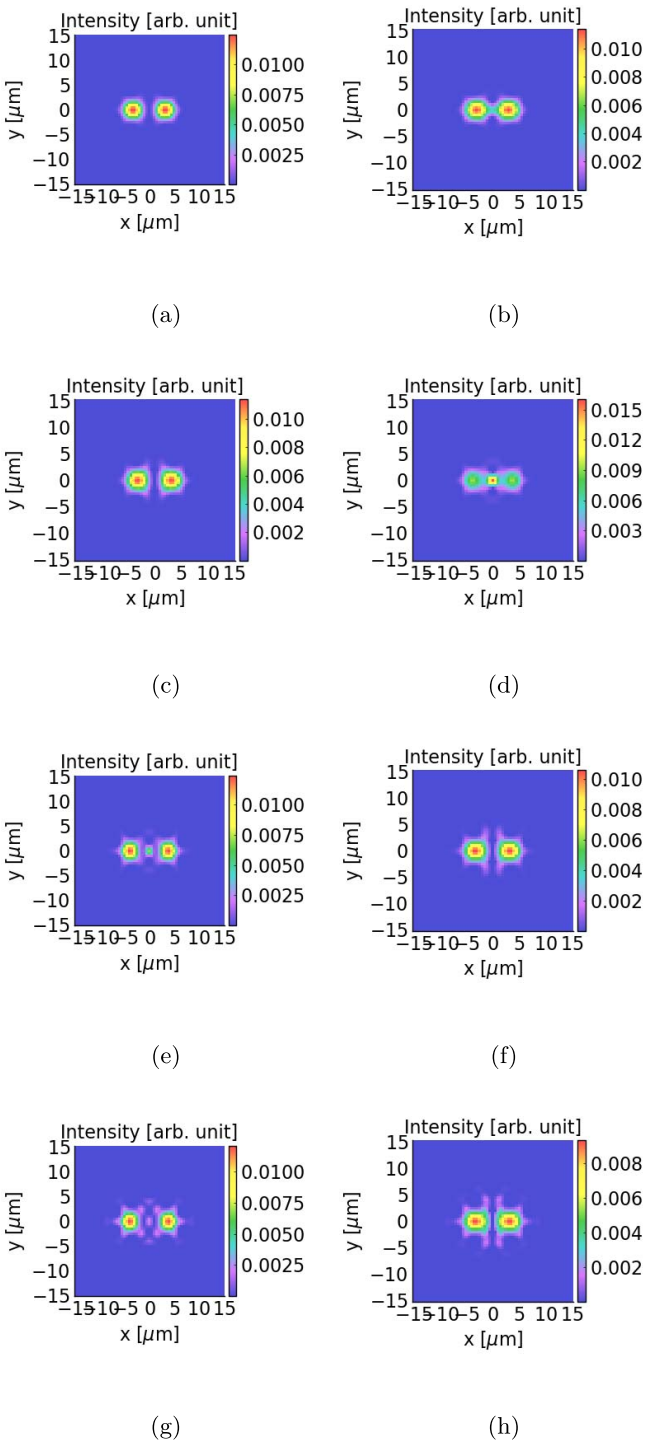

Fig. 12. Modal field intensity profiles for the primary modes (a, c, e, and g) and secondary modes (b, d, f, and h) as a function of index suppression ($n_{\text{suppression}} = [0, 0.0025, 0.0045, 0.007]$).

trends are in agreement with the experimental measurements of Fig. 2b. Moreover, the range of calculated in Fig. 11b are consistent with the experimental measurements in Fig. 2b, 3b, and 4b.

To better understand the evolution of the imaginary component of the coupling coefficient, we can analyze the array supermodes. We solve for the supermode profiles for a series of index suppression values and plot the results in Fig. 12. Note varying the suppression between Fig. 12c- 12d and Fig. 12e-12f (i.e. $0.0025 \leq n_{\text{suppresion}} \leq 0.0045$) we can observe the dominant supermode switches from out-of-phase to in-phase. Comparing Fig. 11b to Fig. 12 we find that the transition of the dominant supermode is associated with the decreased value of $|\kappa_i|$. The switch of the dominant supermode would naturally be expected to occur at low values of mode suppression ratio, which is consistent with the observations of the peak ratio in Fig. 6a.

Finally, the real component of the calculated coupling coefficient in Fig. 11a ranges from tens to 100 GHz. The real coupling coefficient is related to the frequency detuning between the supermodes [7]. Due to limitations of our model, these values should be considered approximate. The supermode dynamics in dual-element photonic crystal arrays have been shown to lead to increased small signal modulation [1] as well as enhanced data transmission rates [3].

VI. Conclusion

Semiconductor lasers have significantly evolved over the course of the illustrious career of Prof. P. D. Dapkus, due in no small part to the impact of his research. The results reported herein would not have been possible without his prior contributions to optoelectronic device physics, semiconductor materials, and the technology used to epitaxially grow the requisite heterostructures.

In this work we use optical power enhancement analysis to estimate the imaginary coupling coefficient for a collection of two-element photonic crystal VCSEL arrays. From measurements and complex waveguide analysis, we find strong optical coupling between the elements with approximately equal current injection. Despite variations observed in array behavior, we find a distinct trend of lowered imaginary coupling coefficient as the photonic crystal lattice period is increased, in agreement with complex waveguide modeling. We refine our waveguide model using experimental estimates of imaginary coupling coefficient. Modeling current injection as increased index suppression in the cavities reveals the imaginary coupling coefficient increases with increased current to a relative maximum, and then decreases in agreement with experimental observations. Beam profile analysis shows that this decrease is associated with an array supermode transition.

The refined complex waveguide model allows us to explore the influence of array design and injection on the complex coupling coefficient. Combined with Fourier beam analysis this reveals conditions for reduced imaginary coupling coefficient, or equivalently lower mode suppression ratio, which are operating conditions that are expected to achieve improved modulation bandwidth.

Acknowledgment

The authors thank S. T. M. Fryslie, B. Thompson, M. T. Johnson, Z. Gao, H. Dave, and K. Lakomy for their prior contributions of design, fabrication, and characterization of the photonic crystal VCSEL arrays.

REFERENCES

[1] S. T. M. Fryslie, M. P. T. Siriani, D. F. Siriani, M. T. Johnson, and K. D. Choquette, "37-GHz modulation via resonance tuning in single-mode coherent vertical-cavity laser arrays," *IEEE Photon. Technol. Lett.*, vol. 27, no. 4, pp. 415–418, Feb. 15, 2015, doi: 10.1109/LPT.2014.2376959.

[2] S. T. M. Fryslie *et al.*, "Modulation of coherently coupled phased photonic crystal vertical cavity laser arrays," *IEEE J. Sel. Topics Quantum Electron.*, vol. 23, no. 6, pp. 1–9, Nov. 2017, doi: 10.1109/jstqe.2017.2699630.

[3] H. Dave *et al.*, "Digital modulation of coherently-coupled 2 × 1 vertical-cavity surface-emitting laser arrays," *IEEE Photon. Technol. Lett.*, vol. 31, no. 2, pp. 173–176, Jan. 15, 2019, doi: 10.1109/LPT.2018.2888806.

[4] H. Dave, Z. Gao, S. T. M. Fryslie, B. J. Thompson, and K. D. Choquette, "Static and dynamic properties of coherently-coupled photonic-crystal vertical-cavity surface-emitting laser arrays," *IEEE J. Sel. Topics Quantum Electron.*, vol. 25, no. 6, pp. 1–8, Nov. 2019, doi: 10.1109/jstqe.2019.2917551.

[5] S. T. M. Fryslie, M. T. Johnson, and K. D. Choquette, "Coherence tuning in optically coupled phased vertical cavity laser arrays," *IEEE J. Quantum Electron.*, vol. 51, no. 11, pp. 1–6, Nov. 2015, doi: 10.1109/JQE.2015.2481724.

[6] Z. Gao, M. T. Johnson, and K. D. Choquette, "Rate equation analysis and non-hermiticity in coupled semiconductor laser arrays," *J. Appl. Phys.*, vol. 123, no. 17, May 2018, Art. no. 173102, doi: 10.1063/1.5022044.

[7] H. Dave, Z. Gao, and K. Choquette, "Complex coupling coefficient in laterally coupled microcavity laser diode arrays," *Appl. Phys. Lett.*, vol. 117, no. 4, Jul. 2020, Art. no. 041106, doi: 10.1063/5.0014468.

[8] P. Strzebonski and K. Choquette, "Complex waveguide supermode analysis of coherently-coupled microcavity laser arrays," *IEEE J. Sel. Topics Quantum Electron.*, vol. 28, no. 1, pp. 1–6, Jan. 2022, doi: 10.1109/jstqe.2021.3096167.

[9] P. Strzebonski, H. Dave, K. Lakomy, N. Jahan, W. North, and K. Choquette, "Computational methods for VCSEL array characterization and control," *Proc. SPIE*, vol. 11704, Mar. 2021, Art. no. 117040L, doi: 10.1117/12.2585066.

[10] P. Strzebonski, "Advances in semiconductor laser mode and beam engineering," Ph.D. dissertation, Dept. Elect. Comput. Eng., Phys., Univ. Illinois Urbana-Champaign, Champaign, IL, USA, 2021.

[11] N. Jahan, W. North, P. J. Strzebonski, K. A. Lakomy, and K. D. Choquette, "Extraction of coupling coefficient for coherent 2×1 VCSEL array," in *Proc. Conf. Lasers Electro-Opt.*, 2021, Paper JTh3A.3.

[12] N. Jahan, W. North, P. Strzebonski, and K. D. Choquette, "Supermode switching in coherently-coupled vertical cavity surface emitting laser diode arrays," *IEEE J. Sel. Topics Quantum Electron.*, vol. 28, no. 1, pp. 1–5, Jan. 2022, doi: 10.1109/jstqe.2021.3117236.

[13] P. Strzebonski, W. North, N. Jahan, and K. D. Choquette, "Machine learning analysis of 2×1 VCSEL array coherence and imaginary coupling coefficient," in *Proc. Conf. Lasers Electro-Opt.*, 2021, Paper JTu3A.110.

[14] P. D. Dapkus, "Laser operation of lightly doped and amphoterically doped GaAs," Ph.D. dissertation, Dept. Elect. Comput. Eng., Phys., Univ. Illinois Urbana-Champaign, Champaign, IL, USA, 1970. [Online]. Available: http://hdl.handle.net/2142/76881

[15] R. D. Dupuis and P. D. Dapkus, "Very low threshold $Ga_{(1-x)}Al_xAs$-GaAs double-heterostructure lasers grown by metalorganic chemical vapor deposition," *Appl. Phys. Lett.*, vol. 32, no. 8, pp. 473–475, Apr. 1978, doi: 10.1063/1.90090.

[16] K. D. Choquette *et al.*, "Single mode photonic crystal vertical cavity surface emitting lasers," *Adv. Opt. Technol.*, vol. 2012, pp. 1–8, Feb. 2012, doi: 10.1155/2012/280920.

[17] S. Fryslie, "Modulation of coherently coupled surface-emitting laser arrays: Analysis and applications," Ph.D. dissertation, Dept. Elect. Comput. Eng., Phys., Univ. Illinois Urbana-Champaign, Champaign, IL, USA, Apr. 2017. [Online]. Available: http://hdl.handle.net/2142/97293

[18] M. T. Johnson, D. F. Siriani, M. Peun Tan, and K. D. Choquette, "High-speed beam steering with phased vertical cavity laser arrays," *IEEE J. Sel. Topics Quantum Electron.*, vol. 19, no. 4, Jul. 2013, Art. no. 1701006, doi: 10.1109/jstqe.2013.2244574.

[19] Z. Gao, S. T. M. Fryslie, B. J. Thompson, P. S. Carney, and K. D. Choquette, "Parity-time symmetry in coherently coupled vertical cavity laser arrays," *Optica*, vol. 4, no. 3, p. 323, Feb. 2017, doi: 10.1364/optica.4.000323.

[20] D. F. Siriani and K. D. Choquette, "Implant defined anti-guided vertical-cavity surface-emitting laser arrays," *IEEE J. Quantum Electron.*, vol. 47, no. 2, pp. 160–164, Feb. 2011, doi: 10.1109/JQE.2010.2068278.

[21] Z. Gao, D. Siriani, and K. D. Choquette, "Coupling coefficient in antiguided coupling: Magnitude and sign control," *J. Opt. Soc. Amer. B, Opt. Phys.*, vol. 35, no. 2, p. 417, Jan. 2018, doi: 10.1364/josab.35.000417.

Pawel J. Strzebonski received the B.S. degree in electrical engineering and the M.S. and Ph.D. degrees in electrical and computer engineering from the University of Illinois at Urbana-Champaign, Urbana, IL, USA, in 2016, 2018, and 2021, respectively. His research interests include computational methods for the design and characterization of photonic devices, such as photonic crystal VCSEL arrays and photonic crystal surface emitting lasers.

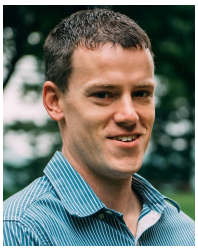

William North received the B.S. degree in electrical engineering from the United States Military Academy (USMA) and the M.S. degree in electrical engineering from Stanford University, CA, USA. He is currently pursuing the Ph.D. degree in electrical engineering with the University of Illinois at Urbana-Champaign. His main research interests are high-speed and high-power photonic crystal VCSEL coupled arrays.

Nusrat Jahan (Graduate Student Member, IEEE) received the B.S. and M.S. degrees in electrical and electronic engineering from the Bangladesh University of Engineering and Technology (BUET). She is currently pursuing the Ph.D. degree in electrical engineering with the University of Illinois at Urbana-Champaign. Her main research interests are characterization and analysis of coherently coupled photonic crystal VCSEL arrays.

Kent D. Choquette (Fellow, IEEE) received the B.S. degree in engineering physics and applied mathematics from the University of Colorado Boulder and the M.S. and Ph.D. degrees in materials science from the University of Wisconsin–Madison. He held a post-doctoral appointment at AT&T Bell Laboratories, Murray Hill, NJ, USA, and then joined Sandia National Laboratories, Albuquerque, NM, USA. In 2000, he joined the Electrical and Computer Engineering Department, University of Illinois at Urbana-Champaign, and is currently the Able Bliss Professor of engineering. He leads the Photonic Device Research Group, which pursues design, fabrication, and characterization of semiconductor vertical cavity surface-emitting lasers, photonic crystal light sources, nanofabrication technologies, and hybrid integration techniques. He has authored more than 300 technical publications as well as presentations at international conferences. He was previously an IEEE Photonics Distinguished Lecturer. He is a fellow of Optica, SPIE, and the American Association for the Advancement of Science. He was awarded the IEEE Photonics Society Engineering Achievement Award, the OSA Nick Holonyak Jr. Award, the SPIE Technology Achievement Award, and the IEEE Photonics Society Distinguished Service Award. He has served in multiple roles at the IEEE Photonics Society, which includes the President from 2016 to 2017.